Journal of Animal & Plant Sciences, 36(2): 2026, Page: 375-390
ISSN (print): 1018-7081; ISSN (online): 2309-8694
https://doi.org/10.36899/JAPS.2026.2.0032

SOIL FERTILITY ASSESSMENT AND MAPPING IN BARDARASH DISTRICT, DUHOK PROVINCE, IRAQ: AN INTEGRATED APPROACH USING GEOSTATISTICS, MACHINE LEARNING, AND LABORATORY ANALYSES

M. A. Salih[1]*, A. V. Bilgili[1] and S. I. K. Rekani[2]

[1] Department of Soil Science, Agriculture Faculty, Harran University, Sanliurfa, Turkiye,
[2] Ministry of Agriculture and Water Resources, Northern region of Iraq
*Corresponding author: moyassar1982@yahoo.com
ORCID ID: 0009-0005-9912-738X

ABSTRACT

Soil fertility is a key determinant of sustainable agricultural productivity, particularly in semiarid regions where conventional surveys are often limited. This study evaluated the fertility status of Bardarash district, Duhok province, Iraq, by developing a soil fertility index (SFI) through an integrative framework combining geostatistical methods, machine learning (ML), GIS, remote sensing, and laboratory analyses. A total of 52 composite soil samples (0-30 cm) were analyzed for 17 physicochemical properties, including texture, bulk density, soil moisture content (SMC), organic matter (OM), soil pH, electrical conductivity (EC), cation exchange capacity (CEC), calcium carbonate ($CaCO_3$), and macro- and micronutrients including available nitrogen (N), phosphorus (P), potassium (K), magnesium (Mg), iron (Fe), manganese (Mn), copper (Cu), zinc (Zn), and boron (B). Principal component analysis (PCA) was applied to assign parameter weights for SFI computation, while ordinary kriging (OK) facilitated the spatial interpolation of soil properties. Additionally, ML techniques, including gradient boosting regression (GBR) and random forest (RF), were employed to enhance soil fertility prediction accuracy. The models were validated using performance metrics such as root mean square error (RMSE), mean absolute error (MAE), mean squared error (MSE), and the coefficient of determination (R^2). The results indicate that GBR achieved the highest predictive accuracy, outperforming both RF and OK. Spatial analyses revealed that approximately 70% of the study area exhibits low fertility, with OM depletion, N and P deficiency, and suboptimal CEC identified as key limiting factors. In order to promote precision agriculture and sustainable land management practices in northern Iraq, these findings emphasize the significance of combining multivariate weighting approaches with geospatial ML and remote sensing to create precise, site-specific soil fertility maps.

Keywords: Soil fertility index, Machine learning, Ordinary kriging, Geographic information systems, Bardarash district

Published first online December 25, 2025 Published final February 28, 2026

INTRODUCTION

Soil fertility ensures that plants receive the essential macronutrients and micronutrients required for healthy growth. Although low soil fertility results in stunted crop growth, reduced yields, and economic losses, excessive nutrient inputs can also lead to nutrient imbalances, lower productivity, and severe environmental consequences, including eutrophication, greenhouse gas emissions, and soil degradation (Lal, 2021; Xing *et al.,* 2025). Additionally, the inefficient or unsustainable exploitation of soil resources accelerates land degradation, jeopardizes ecosystem services, and exacerbates long-term environmental consequences (Kopittke *et al.,* 2025). These challenges underscore the urgent necessity for innovative, data driven, and scalable approaches to soil fertility assessment and management as global agriculture endeavors to achieve sustainable intensification in the face of climate change and resource constraints (Zhou *et al.,* 2022; Zhang and Zhu, 2023; Kumar *et al.,* 2025).

A contemporary and integrative approach for precisely evaluating soil characteristics, enhancing land management, and advancing sustainable agriculture is offered by combining the SFI and ML (Louzada *et al.,* 2025). For instance, remote sensing and GIS have been used to estimate the pH and the EC of the soils on a large scale (Singh *et al.,* 2021). Fuzzy logic and digital mapping have been used to define fertility zones (Keshavarzi *et al.,* 2020), while portable artificial intelligence (AI)- based sensors like handheld X-ray Fluorescence (XRF) have been adopted for quick nutrient assessment (Morais *et al.,* 2021). The significance of integrating geostatistical analysis, GIS, and remote

sensing with ML techniques to enhance the precision of soil fertility prediction and mapping has been underscored by recent advancements in soil fertility research (Zhou *et al.,* 2020; Li, 2022). The SFI offers a thorough assessment of soil productivity by integrating its physical, chemical, and biological characteristics (Askari and Holden, 2015; Rodrigues *et al.,* 2021). This classification enables the delineation of fertility zones, which in turn enables site specific management and precision fertilization strategies (Adhikari *et al.,* 2019). In comparison to conventional statistical methods, ML algorithms, particularly RF and GBR, have exhibited superior predictive capabilities (Zeraatpisheh *et al.,* 2020). Modern technologies, such as digital elevation models (DEMs), satellite imagery, and visible near infrared (VNIR) spectroscopy, provide rapid and cost-effective alternatives to laboratory analyses for the estimation of critical soil parameters, including pH, CEC, and OM (Wang *et al.,* 2023). The accuracy of soil fertility maps is improved and sustainable land management and precision agriculture are supported by the integration of spectral, topographic, and climatic variables with GIS and ML (Gökmen *et al.,* 2023).

The Bardarash District of Duhok, Iraq, remains underserved by comprehensive studies that synthesize geostatistics, GIS, remote sensing, and ML within an integrated SFI framework, despite notable global advancements in this domain. This discrepancy underscores the necessity for a data-driven approach to promote sustainable land management and improve crop productivity in the region. In this study, robust ML algorithms (RF and GBR) and geostatistical interpolation (OK) were utilized to produce high resolution predictions of soil fertility through the integration of geospatial, spectral, and laboratory datasets. The resultant maps aim to identify key fertility limitations, enhance agricultural productivity, and offer actionable insights for sustainable land use planning in northern Iraq. The aims of this research are to assess the predictive accuracy of VNIR spectroscopy, remote sensing data, and laboratory analyses in estimating key soil fertility parameters, employing a comprehensive range of statistical performance metrics. The results of this study are anticipated to enhance scientific knowledge of soil fertility variability, identify principal fertility constraints affecting agricultural productivity, and ultimately promote sustainable land-use planning and informed agricultural decision-making within the region.

MATERIALS AND METHODS

The study location: This study was conducted on agricultural lands in Bardarash district, Duhok, Northern Iraq (36°18′– 37°20′ N; 42°20′–44°17′ E), at 233-485 m altitude. The district covers about 96,097 ha, of which ~76,394 ha is arable according to the Directorate of Agriculture, Bardarash (Figure 1). The landscape is mainly semi-flat, with some non-arable slopes and mountainous areas excluded from sampling. The climate is semi-arid, with an average annual precipitation of ~486 mm concentrated between November and April, and a mean annual temperature of 26.6 °C, ranging from summer maxima of 43 °C to winter minima of -3 °C (General Directorate of Meteorology, Duhok).

Soil sampling and laboratory analysis: A preliminary survey was conducted to determine the locations from which samples would be taken. After excluding areas unsuitable for agriculture, valleys, mountains and inhabited lands, the samples were randomly distributed across the remaining area based on the shape and extent of the land surface, obstacles to sample taking, and other factors. A total of 52 soil samples (0–30 cm) were collected, and each of these 52 samples was as follows: A sample was taken from the previously specified location, then four other samples were taken around this sample from the four directions, at a distance of about 1 km in each direction. Then these five samples were mixed together to form a composite sample that is more accurate and representative of the location. Net samples were air-dried, sieved (2 mm), and analyzed at the Central Laboratory of the University of Mosul following standard procedures (Rekani *et al.,* 2022). The analyses included soil texture, bulk density, SMC, OM, pH, EC, $CaCO_3$, CEC, and available nutrients (N, P, K, Mg, Fe, Zn, Mn, Cu, and B). In addition, hyperspectral reflectance was measured using a FieldSpec Pro sensor across the 350–2500 nm wavelength range.

Soil Fertility Index (SFI) and its Calculation: The SFI was calculated by identifying key soil properties and assigning weights based on their contribution to fertility. Data were normalized to a 0–1 scale using:

$$Ni = \frac{Xi - Xmin}{Xmax - Xmin} \quad (1)$$

Where *Ni* represents the normalized value of the parameter, xi is the raw value of the parameter, and *Xmin* and *Xmax* indicate the minimum and maximum values for that parameter within the dataset. Weighted values were then combined as:

$$SFI = \sum(Wi \cdot Ni) \quad (2)$$

Where *Wi* is the weight of each parameter derived from PCA, which reduced dimensionality and emphasized major variations (Pedregosa *et al.,* 2011; Jolliffe, 2011). The index values close to 0 indicate low fertility, while those near 1 reflect high fertility (Zhang *et al.,* 2018).

Geostatistical and Machine Learning Analysis: Spatial variability of soil parameters was assessed using semivariograms and modeled with OK in ArcGIS 10.5 (Webster and Oliver, 2007; Singh *et al.,* 2010). The degree of spatial dependence (DD) was calculated following Cambardella *et al.* (1994), where values <25%

indicate strong, 25–75% moderate, and >75% weak dependence. To estimate the SFI, two ML algorithms RF and GBR were trained using soil spectral reflectance data across the UV, blue, green, red, and near-infrared (NIR1 and NIR2) spectral regions. These spectral bands were chosen due to their ability to detect variations associated with OM, SMC, mineral composition, and surface reflectance, all of which are closely linked to soil fertility. Prior to modeling, the dataset was pre-processed through the removal of outliers and the handling of missing values to maintain data integrity. The processed dataset was subsequently partitioned randomly into a training subset (80%) for model development and a testing subset (20%) for independent validation. Model accuracy was assessed using standard regression metrics; RMSE and MSE gauge the magnitude of prediction errors, MAE measures the average absolute deviation between predicted and observed values, and R^2 reflects the proportion of variance in SFI accounted for by the model. Reduced RMSE, MAE, and MSE values, along with higher R^2 values, indicate improved predictive accuracy.

Statistical Analysis: Descriptive statistics (minimum, maximum, mean, standard deviation, coefficient of variation, skewness, and kurtosis) were calculated to assess data distribution (Webster, 2001). Normality was tested using the Kolmogorov–Smirnov test ($p > 0.05$), as deviations from normality can affect geostatistical analyses (Kerry and Oliver, 2007). Pearson's correlation coefficients were applied to examine relationships among variables at a significance level of $p < 0.05$. All analyses were performed using SPSS software (version 9.3).

RESULTS

Laboratory and Statistical Evaluation of Soil Physical Parameters: As illustrated in Table 1, the examination of soil qualities revealed substantial variation in critical properties, including bulk density, SMC, sand, silt, and clay content. The sediment content ranged from 26.05 to 85.05%, with a mean result of 42.84%. Conversely, the silt concentration composition ranged from 2.00 to 45% (mean 26.16%), while the clay concentration ranged from 12.95 to 51.45% (mean 31.00%). The bulk density ranged from 1.22 to 1.72 g cm^{-3}, with a mean of 1.43 g cm^{-3}. The average SMC was 17.66%, with a range of 11.13% to 22.59%. The descriptive statistics (Min, Max, Mean, StD, Skewness, Kurtosis, CV, and P-values) are summarized in Table 1. Silt exhibited the maximum dispersion CV = 34.45%, followed by sand 29.69%, clay 27.72%, SMC 16.32%, and bulk density 8.05%.

Laboratory and Statistical Assessment of Soil Physical Properties: Table 1 summarizes the descriptive statistics of the soil physical parameters, indicating significant variation in bulk density, SMC, and particle-size distribution. Sand content ranged from 26.05% to 85.05%, with a mean of 42.84%. Silt content varied from 2.00% to 45%, averaging 26.16%. Clay content ranged between 12.95% and 51.45%, with a mean of 31.00%. Bulk density ranged from 1.22 to 1.72 g cm^{-3} (mean 1.43 g cm^{-3}), while SMC varied between 11.13% and 22.59% (mean 17.66%). The coefficients of variation demonstrated moderate to high variability among the texture fractions, with the greatest dispersion observed in silt, followed by sand and clay.

Table 1. Descriptive statistics of soil physical properties in Bardarash district.

Soil properties	Min	Max	Mean	StD	Skew	Kurt	CV (%)	P-value
Sand (%)	26.05	85.05	42.84	12.72	1.18	1.58	29.69	0.28
Silt (%)	2.00	45	26.16	9.01	-0.51	0.51	34.45	0.41
Clay (%)	12.95	51.45	31.00	8.59	0.17	-0.48	27.72	0.47
Bulk Density (g cm^{-3})	1.22	1.72	1.43	0.11	0.29	-0.54	8.05	0.81
SMC (%)	11.13	22.59	17.66	2.88	-0.16	-0.93	16.32	0.25

Min= Minimum, Max= Maximum, StD= Standard Deviation, Skew= Skewness, Kurt= Kurtosis, CV= Coefficient of Variation
Normality assessments (Kolmogorov–Smirnov) indicated no significant departures from normal distribution assumptions (minimum P = 0.25 for SMC).

Spatial Distribution of Soil Physical Parameters: Figures 2 and 3 illustrated the spatial distribution of soil physical parameters, including bulk density, SMC, and soil texture (sand, silt, and clay). These variations were influenced by the prevailing topographical features. In the southern part of the study area, higher sand content signified soils that were well-drained but typically showed reduced productivity. Conversely, soils with higher silt content provided a better balance between water retention and drainage, which made them more suitable for agricultural cultivation.

Conversely, Figure 3 depicted higher levels of clay content in the eastern and northern regions. Clay-rich soils had better CEC and water retention qualities, which could have enhanced soil fertility.

Laboratory and Statistical Evaluation of Soil Chemical Parameters: Descriptive statistics and laboratory analyses of the soil chemical parameters included minimum, maximum, mean, standard deviation

(StD), skewness, kurtosis, coefficient of variation (CV%), and P-values (Table 2). These statistical measures indicated that the soils chemical properties varied substantially across several parameters.

OM content ranged from (0.20 to 2.79%), with a mean of (1.42%) and StD of (0.69%). The skewness (0.18) indicated an approximately symmetrical distribution, and the kurtosis value -1.008 suggested a platykurtic form. The CV was (48.84%). According to FAO (1980) classes, the soils were distributed as 23% medium, 35% very low, and 42% low. The P-value (0.38) indicated normal data distribution.

Soil pH ranged from (7.15 to 7.51), with a mean of (7.33 ± 0.01) and a StD of (0.076). Skewness (-0.17) and kurtosis (0.11) values indicated a near normal distribution. The CV was (1.04%), and normality was also supported by the P-value (0.92). Based on Jackson (1973), 23% of soils were neutral, and 73% mildly alkaline.

EC (1:1 soil–water suspension at 25°C) ranged between (0.12 and 0.59 dS m^{-1}), with a mean of (0.32 ± 0.012 dS m^{-1}). Skewness (0.39) indicated slight right skewing, while kurtosis (0.71) reflected a slightly peaked distribution. The P-value (0.76) suggested normality, and the CV was (27.67%). According to Durand (1983), all soils were classified as non-saline.

CEC ranged from (12.22 to 31.70 $cmol^{+}$ kg^{-1}), with a mean of (24.50) and a StD of (4.88). Skewness (-0.35) indicated slight left skewing, and kurtosis (-0.78) reflected a platykurtic distribution. The P-value (0.0005) showed deviation from normality. The CV was (19.91%). Based on Durand (1983), 52% of soils had high CEC, and 48% had medium CEC. Spatial patterns of OM, pH, and EC across the study area are presented in Figure 4.

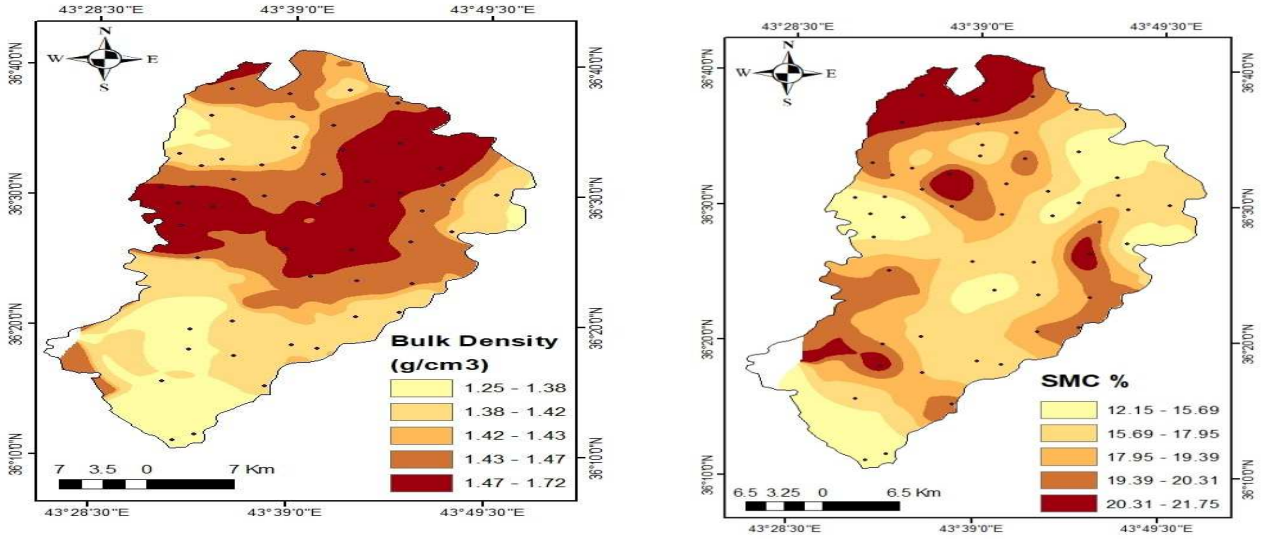

Figure 1. Spatial distribution of Bulk density, and SMC in Bardarash district.

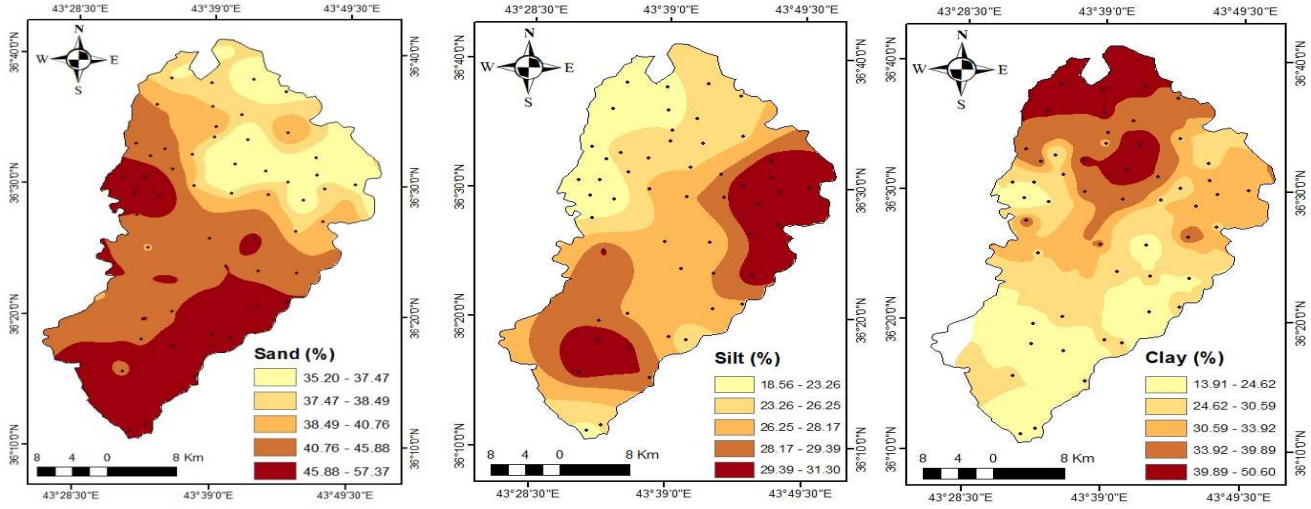

Figure 2. Spatial distribution of soil particles (sand, silt, and clay) in Bardarash district.

Table 2. Dscriptive statistics of soil chemical properties in Bardarash district.

Soil properties	Min	Max	Mean	StD	Skewness	Kurtosis	CV (%)	P-value
OM (%)	0.2	2.79	1.42	0.69	0.18	-1.008	48.84	0.38
Soil pH	7.15	7.51	7.33	0.076	-0.17	0.11	1.04	0.92
EC (dS cm^{-1})	0.12	0.585	0.32	0.089	0.39	0.710	27.67	0.76
CEC (Cmol+ kg-1)	12.22	31.7	24.50	4.88	-0.35	-0.78	19.91	0.0005
$CaCO_3$ (%)	9.00	45.00	28.14	9.23	-0.34	-0.64	32.82	0.81
Avail. N (%)	0.0029	0.0078	0.0054	0.001	-0.15	-0.74	23.25	0.09
Avail. P (ppm)	1.05	8.95	3.65	2.18	1.09	0.27	59.71	0.02
Exch. K (ppm)	28	288	138.76	56.18	0.38	0.81	40.48	0.32
Exch. Mg (ppm)	12.9	22.4	18.14	2.05	-0.24	0.69	11.32	0.78
Exch. Fe (ppm)	2.72	97.5	36.05	30.80	0.79	-1.005	85.42	0.00
Exch. B (ppm)	0.104	8.84	1.16	1.33	4.27	22.01	114.86	0.00
Exch. Cu (ppm)	1.00	9.16	3.76	1.94	0.92	0.44	51.57	0.53
Exch. Zn (ppm)	10.00	99.7	59.44	25.06	-0.28	-0.84	42.17	0.78
Exch. Mn (ppm)	1.05	9.87	4.82	1.99	-0.0017	-0.46	41.27	0.47

Min= Minimum, Max= Maximum, StD= Standard Deviation, Skew= Skewness, Kurt= Kurtosis, CV= Coefficient of Variation

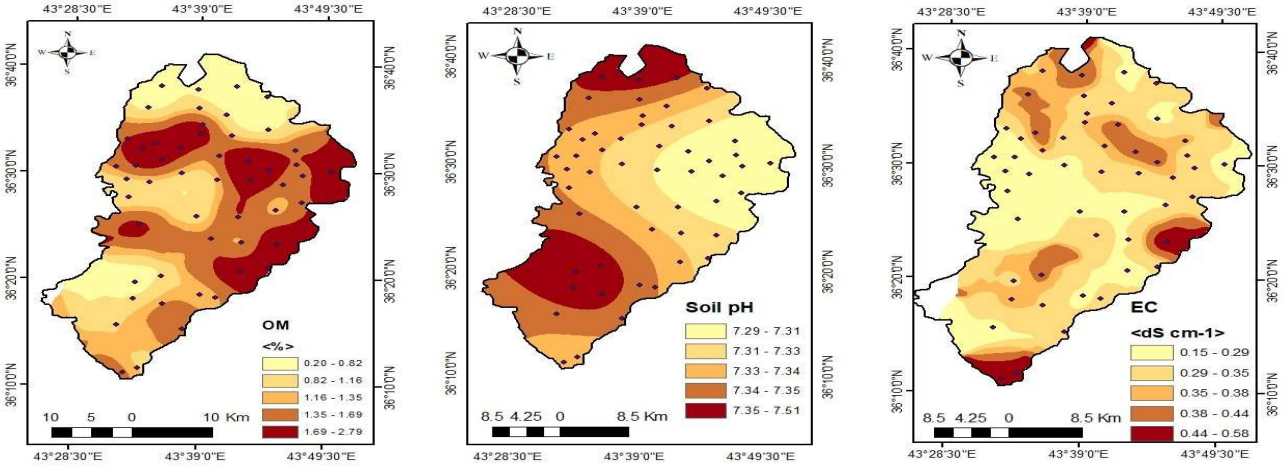

Figure 3. Spatial distribution of soil OM, pH, and EC in Bardarash district.

The $CaCO_3$ content varied between 9% and 45%, with an average of 28.14%. The distribution exhibited a minor left skew skewness (-0.34) and was platykurtic kurtosis (-0.64). The CV was (32.82%), signifying substantial variability. The P-value (0.81) suggested a normal distribution. According to Belay *et al.* (2025), 94% of the soils were categorized as high to very high in $CaCO_3$, while 6% were classified as medium. Figure 5 illustrates the spatial distributions of $CaCO_3$ and CEC.

Available N ranged from (0.0029% to 0.0078%), with a mean of (0.0054%). The distribution was marginally negatively skewed skewness (-0.15) and exhibited platykurtic characteristics kurtosis (-0.74). The CV was (23.25%), and the P-value (0.088) indicated approximate normality. According to Counties (2010), 94% of the soils were categorized as having very high levels of available nitrogen, whereas 6% were classified as high. Available P ranged from (1.05 to 8.95 ppm), with a mean of (3.65 ppm) and a StD of (2.18 ppm). The distribution exhibited positive skewness (1.09) and mild leptokurtosis (0.27). The P-value (0.021) suggested a statistically significant departure from normality. The CV was (59.71%), reflecting considerable variability. According to Matar (1992), 48% of soils exhibited very low levels of phosphorus, 46% were low, and 6% were medium.

Available K levels ranged from (28 to 288 ppm), with a mean of (138.76 ppm) and a StD of (56.18 ppm). The data demonstrated a minor right skewness of (0.38) and a moderate kurtosis of (0.81). The P-value (0.32) suggested a normal distribution. The CV was (40.48%), indicating moderate variability. Available Mg levels ranged from (12.9 to 22.4 ppm), with a mean of (18.14 ppm) and a StD of (2.05 ppm). The distribution exhibited a modest left skewness (skewness -0.24) and a kurtosis of 0.69. The P-value (0.78) suggested normality. The CV was 11.32%, indicating limited variability. Spatial distribution maps of soil macronutrients (N, P, K, Mg)

were generated employing ordinary kriging, as illustrated in Figure 6.

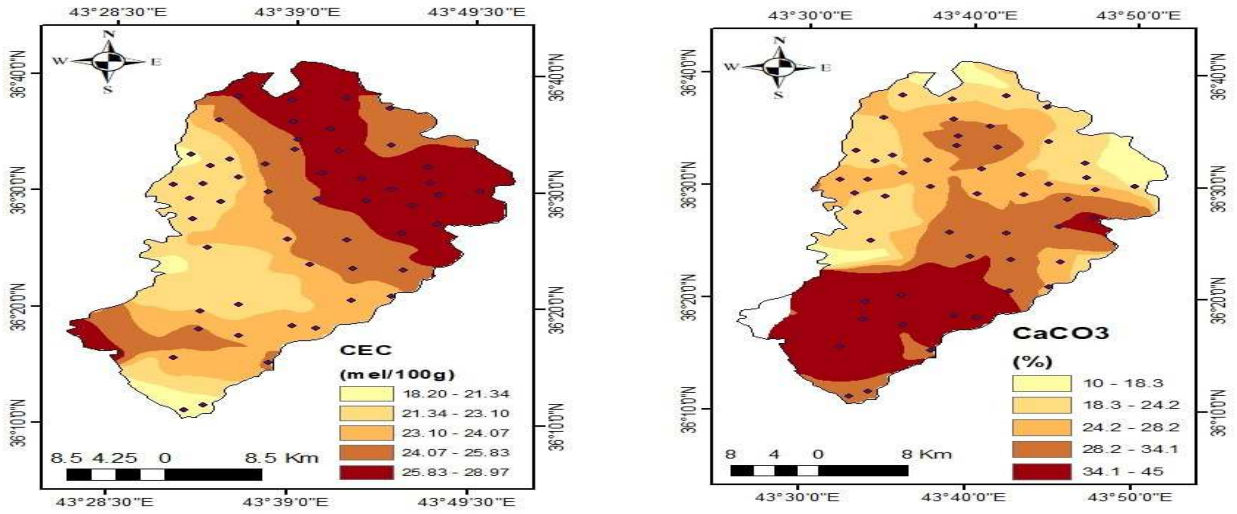

Figure 4. Spatial distribution of CEC and $CaCO_3$ in Bardarash district.

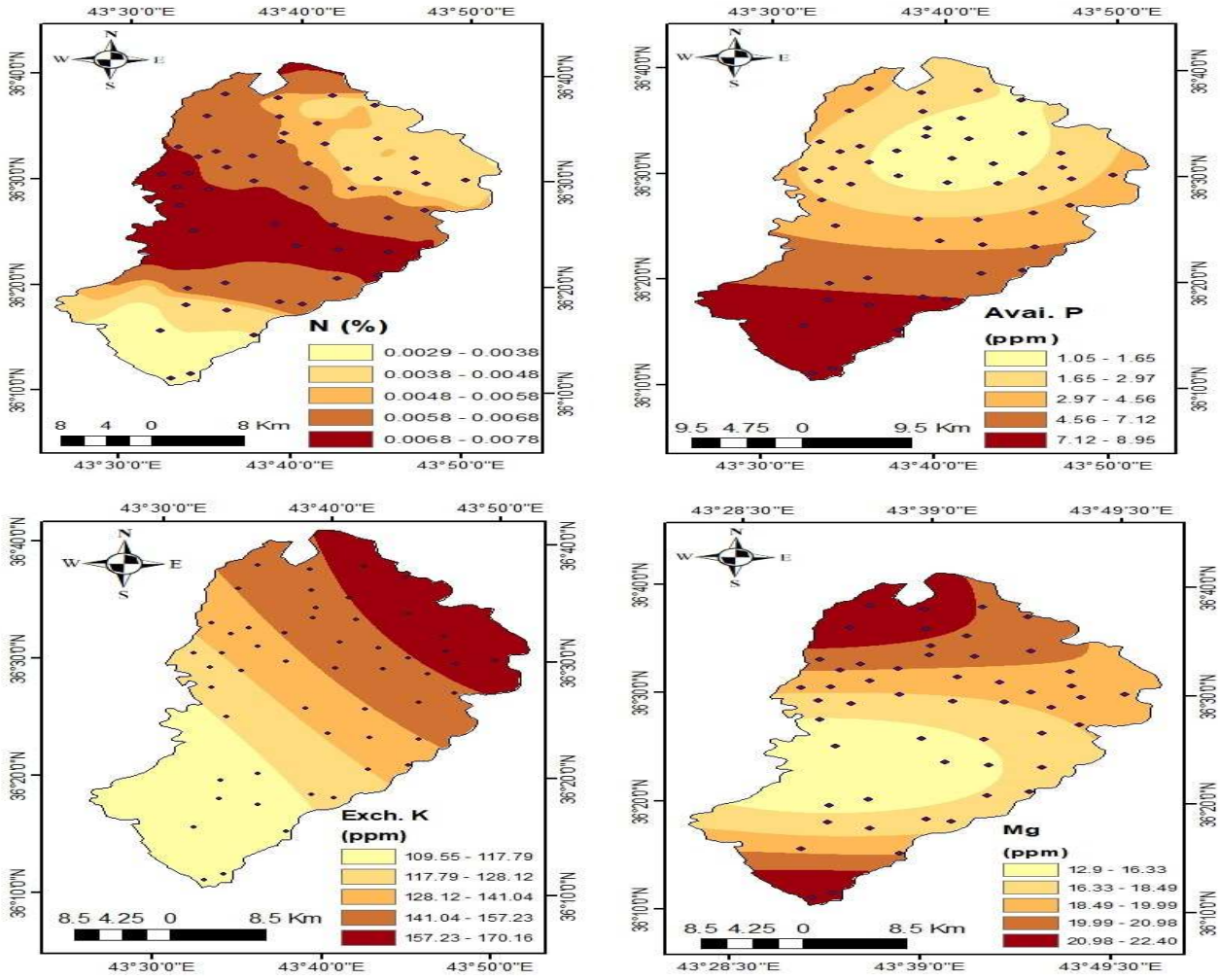

Figure 5. Spatial distribution of soil macronutrients (N, P, K and Mg) in Bardarash district.

Micronutrients: Iron levels ranged from (2.7 to 97.5 ppm), with a mean of (36.05 ppm) and a StD of (30.80 ppm). The distribution exhibited right skewness (0.79) and platykurtic kurtosis (-1.01). The CV was (85.42%), and the P-value (0.00027) indicated a significant departure from normality. B ranged from (0.10 to 8.84 ppm), with an average of (1.18 ppm). The data exhibited significant right skewness (4.27) and pronounced leptokurtosis kurtosis (22.01). The CV was (114.86%), and the P-value (0.0015) suggested a non-normal distribution. Cu levels ranged from (1.0 to 9.16 ppm), with a mean of (3.76 ppm) and a StD of (1.94 ppm). A slight right skewness (0.92) and modest kurtosis (0.44) were observed. The P-value (0.53) suggested normality. The CV amounted to 51.57%. Zn concentrations ranged from (10.0 to 99.7 ppm), with a mean of (59.44 ppm) and a StD of (25.06 ppm). The distribution exhibited moderate variability CV (42.17%), was mildly left-skewed (-0.28), and demonstrated a platykurtic shape (-0.84). The P-value (0.78) suggested a normal distribution. Mn levels ranged from (1.05 to 9.87 ppm), with a mean of (4.82 ppm) and a StD of (1.99 ppm). The distribution was approximately symmetrical skewness (-0.0017) and mildly platykurtic (-0.46). The P-value (0.47) suggests that the data conforms to a normal distribution. The CV was calculated at 41.27%. Micronutrient spatial distribution maps (Fe, Zn, Cu, Mn, B) were produced using the same ordinary kriging employed for macronutrients and were presented in Figure 7.

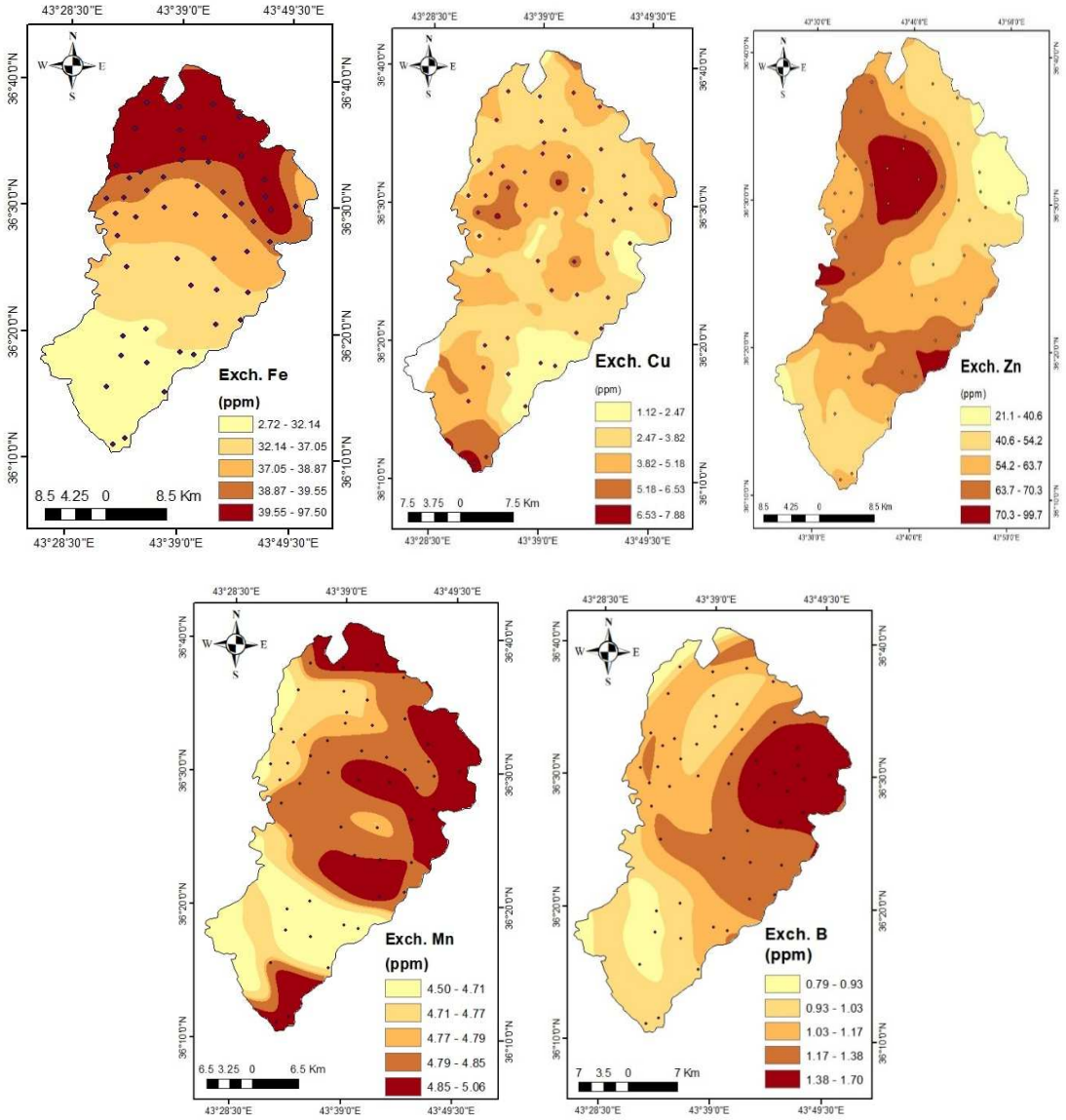

Figure 6. Spatial distribution of soil micronutrients (Fe, Cu, Zn, Mg and B) in Bardarash district.

Semivariogram of Soil Properties: Before the models were selected, the semivariograms were fitted to spherical, exponential, Gaussian, or linear models, and the best fit with matching coefficients of determination (R^2) was visually assessed. Nugget semivariance, range, and sill (total semivariance) were among the model parameters. The sill shows the lag distance beyond which values are no longer spatially connected, whereas nugget semivariance represents both field and experimental variability, displaying variance at zero distance. The range is the distance at which there is no longer any spatial association between variables. Table 3 summarizes the model performance and spatial variability and presents the semivariogram parameters needed to produce OK interpolation for various soil attributes. Significant variance in geographical interdependence among soil properties was revealed by statistical markers as Spatial Dependence (SD %), MAE, RMSE, and R^2. For instance, there was a notable regional dependence in the low nugget-to-sill ratios of OM and accessible Fe.

Table 3. Semivariogram parameters and model error metrics for soil properties in Bardarash district.

Soil Properties	Model	Sill	Nugget	Range	SD (%)	MAE	RMSE	R^2
OM (%)	Spherical	0.518	0.183	8520	35.32	-0.00022	0.499	0.620
Soil pH	Exponential	0.00864	0.00419	40542	48.49	-0.00054	0.508	0.193
EC ($dS\ m^{-1}$)	Gaussian	0.00822	0.00034	2010	4.13	0.001909	0.087	0.684
CEC ($cmol\ (+)\ kg^{-1}$)	Linear	27.42	19.45	25304	70.93	0.115	4.791	0.139
$CaCO_3$ (%)	Spherical	83.08	20.06	1537	24.14	0.182	8.798	0.168
Avail. N (%)	Spherical	0.00003	0.00001	7720	33.33	1.13e-	0.001	0.686
Avail. P (ppm)	Gaussian	4.38	0.16	2226	3.65	-0.0083	2.193	0.683
Exch. K (ppm)	Spherical	2925	1053	4540	36	-0.016	55.74	0.511
Exch. Mg (ppm)	Gaussian	3.76	0.7	1197	18.61	-0.020	2.124	0.509
Exch. Fe (ppm)	Gaussian	951	1.01	2100	0.106	0.688	30.66	0.805
Exch. B (ppm)	Gaussian	2.16	0.001	1391	0.046	0.0305	1.343	0.413
Exch. Cu (ppm)	Gaussian	3.86	0.01	2230	0.25	0.0082	1.980	0.659
Exch. Zn (ppm)	Gaussian	629.5	1.02	2300	0.16	0.615	25.42	0.676
Exch. Mn (ppm)	Linear	6.56	2.79	32551	42.53	0.0066	2.097	0.252
Bulk Density ($Mg\ m^{-3}$)	Gaussian	0.012	0.00001	1920	0.083	0.0004	0.116	0.645
SMC (%)	Gaussian	8.91	0.01	2900	0.11	-0.011	2.747	0.774
Sand %	Exponential	174.36	65.9	6637	37.79	0.0065	12.20	0.328
Silt %	Linear	98.83	83.98	14603	84.97	0.099	9.084	0.186
Clay %	Exponential	68.38	15.8	4530	23.10	-0.077	6.681	0.606

SD%= Spatial dependence, MAE= mean absolute error, RMSE= root mean square error, and R^2= coefficient of determination.

On the other hand, comparatively higher nugget values for soil pH and silt concentration indicated poorer spatial organization. Additionally, the ranges were quite large, ranging from localized values for accessible Mg (1,197 m) and $CaCO_3$ (1,537 m) to widespread values for soil pH (40,542 m) and CEC (25,304 m). The model's performance also varied, with lower R^2 values for soil pH (0.189) and silt content (0.186) reflecting weaker predictions and higher R^2 values for available Fe (0.805) and SMC (0.774) suggesting great predictive accuracy.

Correlation Matrix Between Soil Properties: A dendrogram is presented in Figure 8, which also includes the clustered correlation matrix heatmap, to illustrate the relationships between soil and environmental properties. The dendrogram hierarchically groups variables based on their similarity, while the heatmap displays correlation coefficients that range from (-1 to 1), indicating the strength and direction of associations. The findings indicate that there are distinct clusters of variables that are significantly correlated. For example, the presence of a single cluster containing clay content, CEC, and OM suggests that a higher clay content is typically correlated with higher levels of CEC and OM. Another cluster was composed of nutrient-related variables, including available Mg, Ca, and K, which underscored their interconnection in nutrient availability.

The inverse association between soil fertility indices and factors such as sand content and bulk density was confirmed by the negative correlations observed. The most robust positive correlations were observed between clay content and CEC, as well as between OM and CEC.

Spatial Distribution of Soil Fertility: To evaluate the performance of the applied models, Figure 9 illustrates the cumulative variance and scatter plots that were used to assess the dimensionality reduction and variable contributions. Building on this evaluation, three approaches OK, RF, and GBR were employed to generate soil fertility maps.

The spatial distribution patterns derived from these models are presented in Figure 10, which provides a comparative visualization of fertility status across the study area. Understanding such regional variation is essential for effective land management and sustainable agricultural practices. Based on semivariogram modeling and geographic autocorrelation, OK generated fertility estimates using sill, nugget, and range parameters, as shown in Table 4.

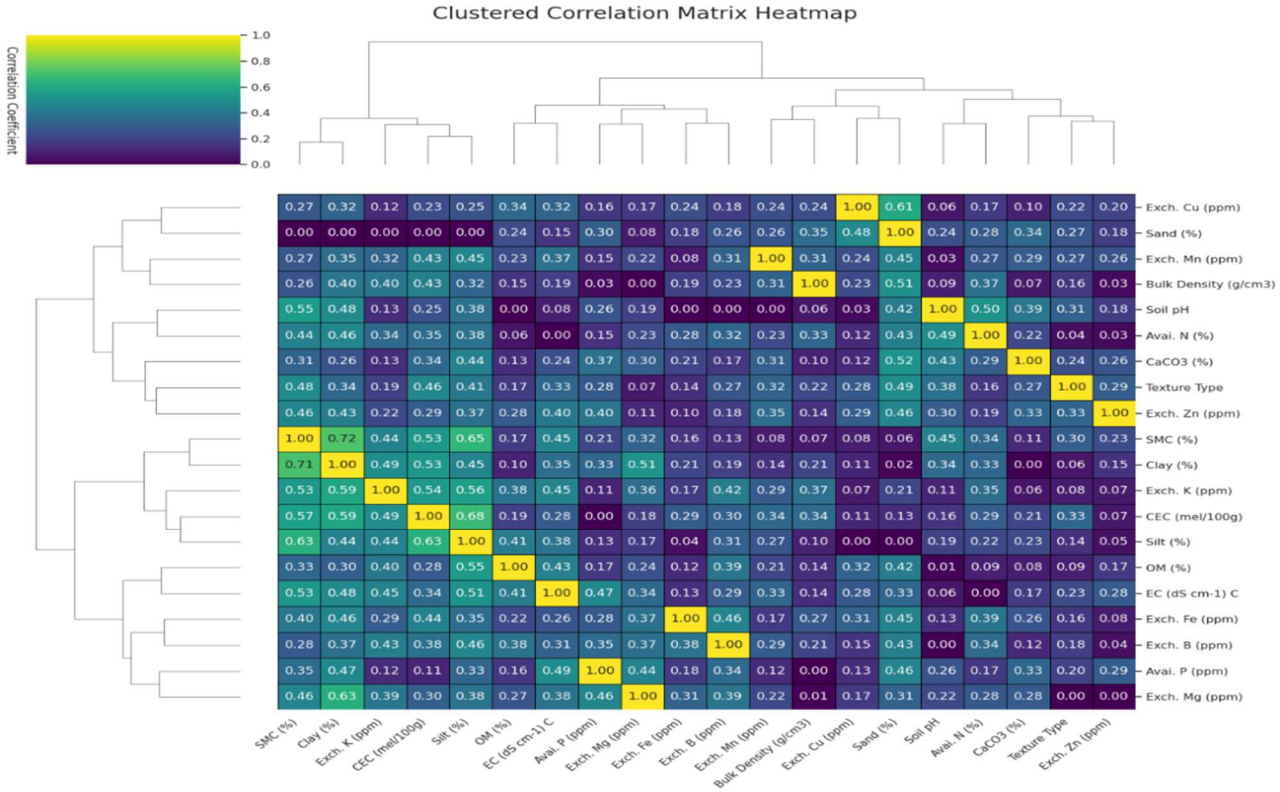

Figure 8. Correlation metric with dendrograms of soil properties.

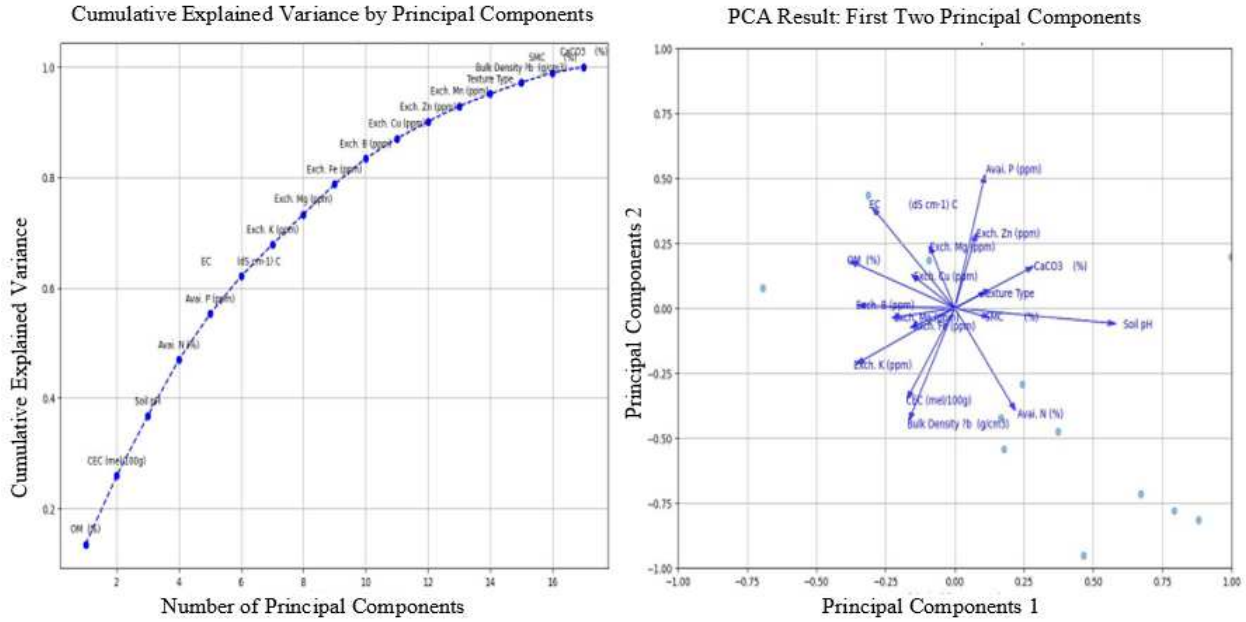

Figure 9. Assigning weight of soil properties by using PCA approach

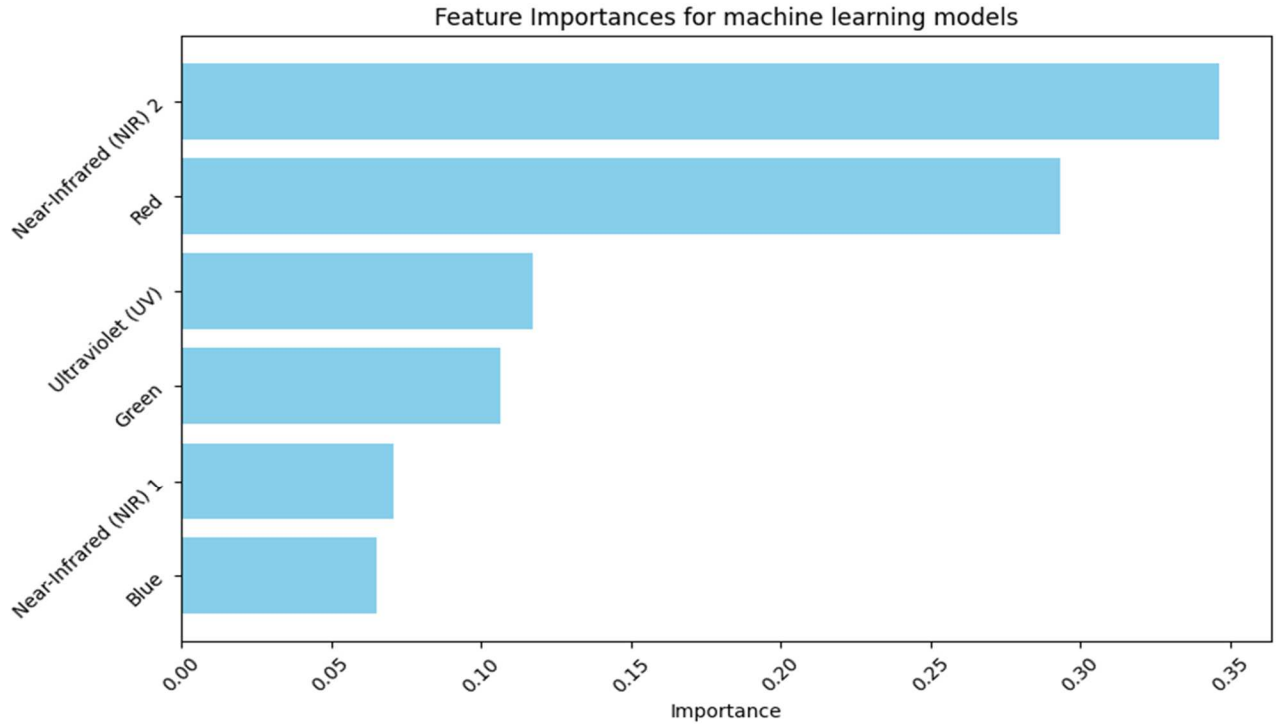

Figure 10. Feature importance of soil properties in predicting SFI using ML models (RF and GBR).

The range (14,603 m) shows the distance of spatial correlation, the sill (0.0072) depicts total variance, and the nugget value (0.0043) indicates unexplained variation that is most likely caused by measurement error or microscale variability (Webster and Oliver, 2007; Cressie, 2015).

Table 3: Semivariogram parameters of Soil fertility index (SFI)

Soil properties	Nugget	Sill	Range	SD %
SFI	0.0043	0.0072	14603	59.72

There are noticeable variations between models in the fertility categorization results (Table 5). OK classified fertility as very low at 520 km^2 (45.5%), low at 497 km^2 (43.5%), and moderate at 125 km^2 (10.09%). 316 km^2 (27.68%), 738 km^2 (64.69%), and 87 km^2 (7.36%) were classified as moderate, low, and extremely low by RF. The GBR forecasted 285 km² (25.11%) as moderate, 781 km^2 (68.84%) as low, and 69 km^2 (6.08%) as very low. The region is dominated by low fertility (68–70%) across all models, however GBR and RF showed more pockets of intermediate fertility than OK.

Table 4: Fertility classes resulted from geostatistical models used

Model	Very low fertility		Low fertility		Moderate fertility	
	Area (km^2)	%	Area (km^2)	%	Area (km^2)	%
Ordinary kriging (OK)	520	45.5	497	43.5	125	10.09
Random forest (RF)	87	7.36	738	64.69	316	27.68
Gradient boosting regression (GBR)	69	6.08	7	781	285	25.11

Additionally, there were differences in the spatial patterns: OK created smoother transitions between fertility zones, with low fertility in the southwest and moderate fertility in the north. GBR produced balanced maps that caught both subtle heterogeneity and seamless transitions, whereas RF produced more fragmented zones with clear borders and fine-scale detail as showed in Figure 11.

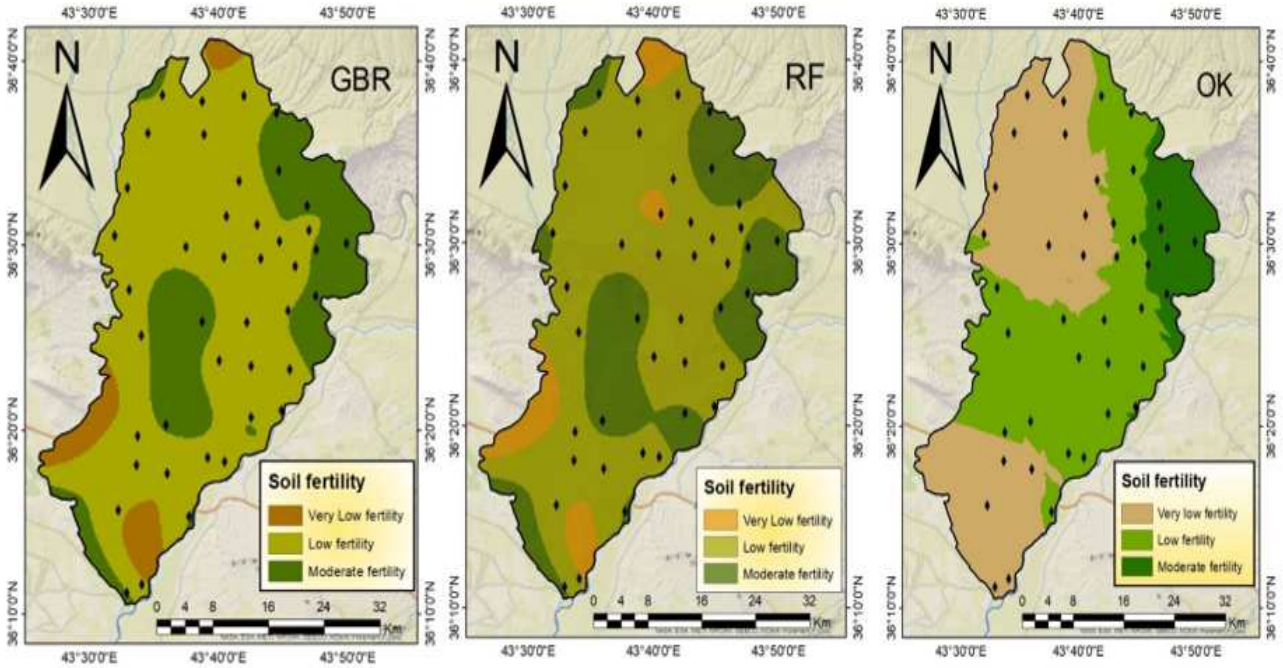

Figure 11. Spatial distribution of soil fertility in Bardarash region, predicted by GBR, RF, and OK.

Accuracy Assessment of Spatial Distribution Models of Soil Fertility: Soil fertility was predicted using three models: OK, RF, and GBR. MAE, MSE, RMSE, and R^2 values were used to assess each model's accuracy (Table 6).

Table 5: Error metrics of ordinary kriging, random forest, and gradient bossing regression

Model	MAE	MSE	RMSE	R^2
Ordinary kriging	0.0428	0.0025	0.0505	0.22
Random forest	0.0184	0.0005	0.0228	0.83
Gradient boosting regression	0.0075	0.0001	0.0087	0.97

With an R^2 value of 0.22, the OK model performed the worst, explaining only 22% of the variation in soil fertility (Isaaks and Srivastava, 1989). Greater differences between actual and anticipated values were corroborated by its higher RMSE (0.0505) and MAE (0.0428). In comparison, the RF model performed noticeably better. It explained 83% of the variation with an R^2 value of 0.83, although reduced prediction errors were suggested by MAE (0.0184) and RMSE (0.0228) values (Breiman, 2001). Both OK and RF performed worse than the GBR model. Its MAE (0.0075) and RMSE (0.0087) values showed exceptionally low prediction errors, and its R^2 value of 0.97 explained 97% of the dataset variation (Friedman, 2001). According to these findings, GBR predicts soil fertility in the study area with the highest accuracy (Figure 12).

Spatial Distribution of Environmental Characteristics and their effects on Soil fertility: Elevation, slope, and aspect are important environmental elements that have a significant impact on soil formation, hydrological processes, and land-use suitability. Figure 13 shows how these characteristics are distributed spatially.

The research area's elevation varied from 193 to 840 meters, with the northern and central zones having the highest values. The local climate, drainage, and vegetation growth were all significantly impacted by these differences. Because of increased runoff and decreased soil stability, steep slopes (23.27° to 70.66°), which are concentrated in higher elevation areas, were shown to be more vulnerable to rapid erosion. Slope values also varied significantly. The gentler slopes (0°-15°) that predominate in the southern zones, on the other hand, are less likely to experience erosion and are better suited for farming because of their easier access and stable soil. Variability in the microclimate was also influenced by aspect. In contrast to south-facing slopes, which had drier soil conditions, faster evaporation, and more solar radiation, north-facing slopes held onto more soil moisture and supported unique vegetation patterns.

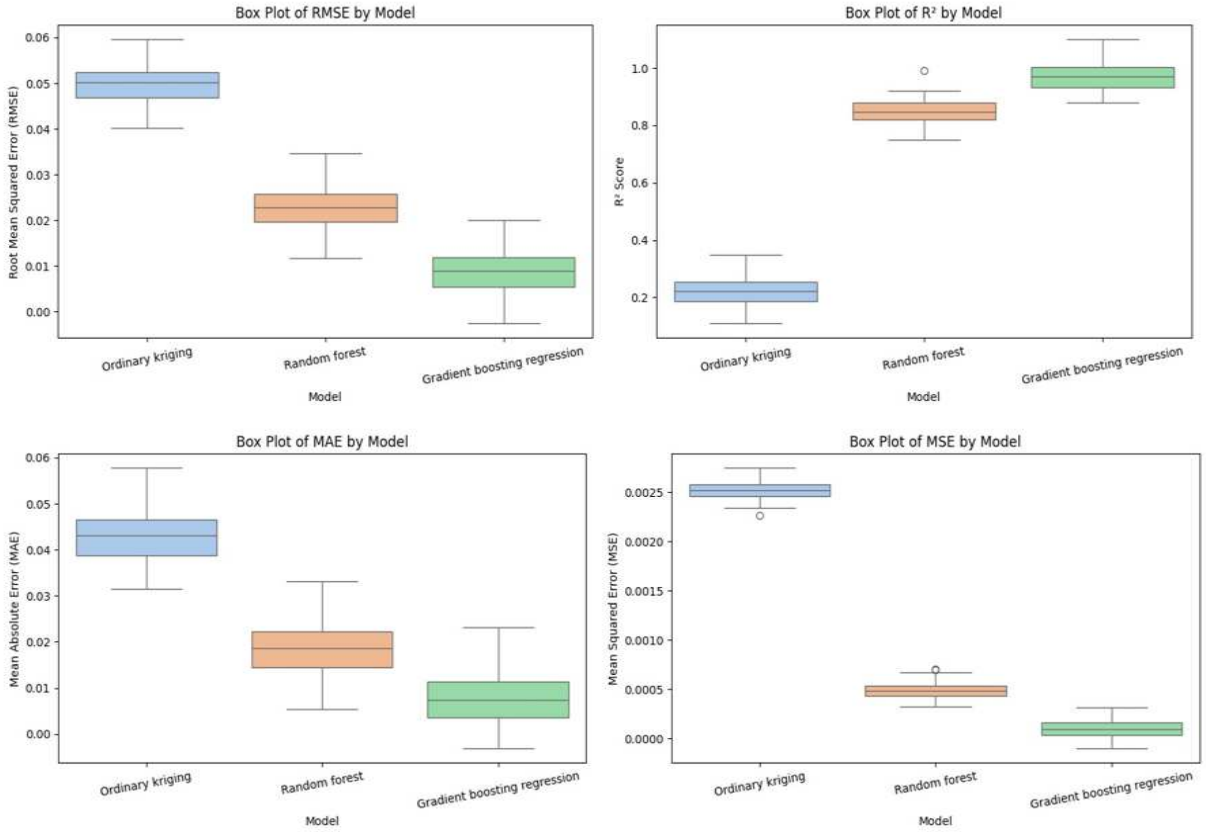

Figure 12. Error metrics (MAE, MSE, RMSE, and R^2) for OK, RF, and GBR.

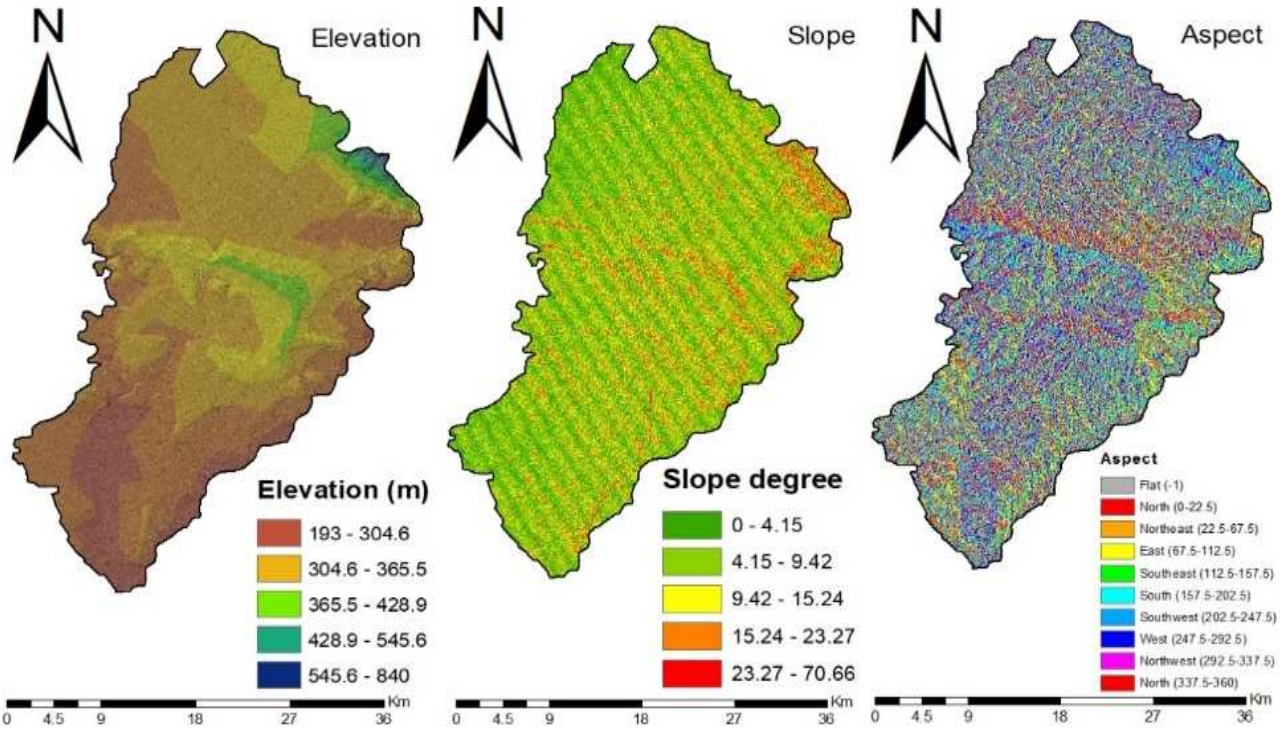

Figure 13. Environmental variable (Elevation, Slope, and aspect) of study region

DISCUSSION

The spatial and statistical distributions of soil properties in the Bardarash district demonstrate a highly heterogeneous environment influenced by parent material, topography, land use, and climatic factors. Soil texture demonstrated significant variability, with silt exhibiting a relatively uniform distribution, while clay and sand exhibited light-tailed and leptokurtic distributions, respectively, indicative of diverse depositional processes and land-use influences (Diaz-Zorita *et al.,* 2004). Because soil composition influences water and nutrient retention (Hillel, 1998), clay-rich regions are likely to retain greater amounts of moisture and nutrients, whereas sandy areas tend to exhibit rapid drainage and leaching characteristic of semi-arid environments (Cui *et al.,* 2023). SMC enhances these textural effects by facilitating nutrient absorption and promoting biomass growth (Hudson, 1994). Nutrient partitioning among particle-size fractions specifically, K and Ca in medium-sized aggregates and P, Mg, and micronutrients in particles smaller than 10 μm (Isaboke *et al.,* 2025) coupled with the increased erodibility of fine particles (Hao *et al.,* 2016), accounts for the observed redistribution across the landscape. Topography exerts a significant influence on soil distribution patterns. Steeper slopes experienced the removal of fine sediments via erosion, resulting in coarser textures and diminished fertility, while lower areas accumulated finer materials and retained moisture, thereby improving nutrient availability (Amare *et al.,* 2024; Zhou *et al.,* 2024). Aspect effects were also observed: north-facing slopes maintained higher levels of moisture and organic matter compared to south-facing slopes, thereby enhancing fertility, in accordance with the findings of (Magdic *et al.,* 2022; Bao *et al.,* 2024). These findings highlight the importance of incorporating terrain characteristics into land-use planning.

Chemical properties exhibited comparable complexity. OM levels were diminished due to elevated temperatures, decreased rainfall, and limited organic inputs, as reported by Fayyadh and Ismail (2021), thereby impairing structural stability and nutrient cycling. Soil pH primarily remained within the optimal range (5.5-7.5), suggesting minimal limitations due to acidity or alkalinity (Landon, 1991; Nigussie *et al.,* 2013). EC values persisted at low levels, indicating a minimal salinity risk (Fattah and Fayyadh, 2019), although ongoing monitoring is advised (Durand, 1983). CEC levels varied from moderate to high, indicating effective nutrient retention (Razvanchy and Fayyadh, 2022). High $CaCO_3$ levels associated with carbonate-rich parent material and arid conditions (Fayyadh and Rekani, 2022) contributed to phosphorus fixation, further exacerbated by low OM, elevated temperatures, and limited precipitation (Singh *et al.,* 2010), rendering phosphorus the most limiting nutrient in Bardarash.

N availability varied geographically as a result of management practices and historical cultivation patterns, with increased nitrogen levels promoting soil structure improvement through enhanced organic matter decomposition and nitrification (Khudher and Alkhaled, 2024). K was predominantly deficient due to root depletion and soil mineral composition, whereas Mg levels remained consistently elevated, negating the necessity for Mg fertilization. Micronutrients (Fe, Zn, Cu, Mn) were adequate, whereas B exhibited localized variability; these findings are consistent with (FAO, 1980; Soltanpour, 1985; Johnson and Fixen, 1990). Correlation patterns emphasize the fundamental importance of OM: its robust relationships with clay and sediment underscore its impact on nutrient retention, aggregation, and cation exchange capacity (Brady and Weil, 2017; Lal, 2021). The inverse correlation between bulk density and OM corroborates enhanced soil structure resulting from OM enrichment (Six *et al.,* 2000). These relationships highlight the significance of organic matter management, especially the application of organic amendments and cover crops (Jones and Jacobsen, 2005).

ML models (RF and GBR) surpassed OK in forecasting soil fertility owing to their capacity to capture nonlinear and spatially intricate interactions. Although OK demonstrates strong performance in datasets with significant spatial dependence (Webster and Oliver, 2007), RF and particularly GBR exhibited superior predictive accuracy, corroborating findings by (Rodriguez-Galiano, 2012; Vaysse *et al.,* 2017). The robust performance of GBR highlights its appropriateness for precision agriculture that necessitates detailed fertility mapping. Overall, the integration of laboratory data, geostatistics, and machine learning offers a comprehensive understanding of fertility limitations in Bardarash. The significant variability in OM, P, Ca CO_3, and CEC underscores the importance of implementing site-specific nutrient management, precision fertilization, and organic matter improvement to promote sustainable agriculture within the semi-arid regions of northern Iraq.

Conclusions: The results of this study indicate that soil fertility in the Bardarash district is primarily constrained by low organic matter (OM) content significant phosphorus (P) deficiency, and elevated calcium carbonate ($CaCO_3$) levels, all of which impede nutrient availability and overall soil productivity. The evident spatial heterogeneity of these properties underscores the intricate interactions among parent material, topography, climate, and land-use practices. Machine learning (ML) models, especially Gradient Boosting Regression (GBR), demonstrated higher predictive accuracy in modeling the nonlinear and spatial heterogeneity of soil fertility relative to conventional geostatistical methods. These

findings highlight the significance of integrating laboratory analyses with sophisticated data-driven methods to enhance the precision of fertility evaluations. Overall, the study offers a robust scientific basis for instituting site-specific nutrient management, increasing organic matter inputs, and applying phosphorus-centered fertilization to promote sustainable agricultural practices in the semi-arid regions of Bardarash.

Author contributions: All authors contributed equally to the concept idea and design of the study. All authors have read and agreed to the published version of the manuscript.

Conflicts of interest: All of the authors declare that there is no conflict of interest regarding the publication of this paper.

Data availability statement: Some or all data, models, or code that support the findings of this study are available from the corresponding author.

Funding: This research did not receive any specific grant from funding agencies in the public, commercial, or not-for-profit sectors. All expenses related to this study were covered by the corresponding author.

Conflict of interest disclosure: The authors declare no competing interests.

Permission to reproduce material from other sources: All the materials in this manuscript are original.

REFERENCES

Adhikari K, Hartemink AE, Minasny B, Bou Kheir R, Greve MB, Greve MH (2014). Digital mapping of soil organic carbon contents and stocks in Denmark. PLoS One, 9(8): e105519. https://doi.org/10.1371/journal.pone.0105519

Amare H, Admase H, Ewunetu T (2024). Influence of land-use types and topographic slopes on the physico-chemical characteristics of soils in Northwestern Ethiopia. Fron. Soil Sci. 4: 1-9. https://doi.org/10.3389/fsoil.2024.1463315

Askari MS, Holden NM (2015). Quantitative soil quality indexing of temperate arable management systems. Soil Tillage Res. 150: 57-67. https://doi.org/10.1016/j.still.2015.01.010

Bao H, Lann T, Ao X, Yang L, Lan H, Peng J (2024). Evolution characteristic of soil water in loess slopes with different slope angles. Geoenviron. Disas. 11(1): 43. https://doi.org/10.1186/s40677-024-00293-6

Belay AM, Selassie YG, Tsegaye EA, Meshesha DT (2025). Comparison of laboratory methods for predicting soil lime requirements of Luvisol in Dera district, the Northwestern highlands of Ethiopia. Tropical Agri. 102(1): 105-123. https://journals.sta.uwi.edu/ojs/index.php/ta/article/view/9059

Brady NC, Weil RR (2017). The Nature and Properties of Soils, 15th edition (eBook).

Breiman L (2001). Random Forests. Machine Learning 45(1): 5-32. https://doi.org/10.1023/A:1010933404324

Cambardella CA, Moorman TB,Novak JM,Parkin TB,Karlen DL,Turco RF,Konopka AE(1994). Field Scale Variability Soil Properties in Central Iowa Soils. Soil Sci. Soc. Amer. J. 58: 1501-1511. https://doi.org/10.2136/sssaj1994.03615995005800050033x

Counties S (2010). *Primary plant nutrients*: Nitrogen, phosphorus and potassium (pp. 4-6). University of California Agriculture and Natural Resources (UCANR).

Cressie N (2015). *Statistics for spatial data.* John Wiley & Sons.

Cui S, Zhu P, Liu P,Geng X (2023). Effects of soil particle structure on the distribution and transport of soil water and salt. Water 15(15), 2842. https://doi.org/10.3390/w15152842

Díaz-Zorita M, Grove JH, Murdock L, Herbeck J, Perfect E (2004). Soil structural disturbance effects on crop yields and soil properties in a no-till production system. Agron. J. 96(6): 1651-1659. https://doi.org/10.2134/agronj2004.1651

Durand JH (1983). *Les sols irrigables; etude pedologique;* Presses Universitaires de France: Paris, France.

FAO (1980). *Soil testing and plant analysis.* Bull. No. 38/1, Food and Agriculture Organization, Rome, Italy.

Fattah SA, Fayyadh MA (2019). Comparison of some soil quality indicators of forest soils under two different tree species. J. Duhok Univ. 22(2):133-146. https://doi.org/10.26682/ajuod.2019.22.2.13

Fayyadh, MA, Ismail HK (2021). genesis, development, and classification for some selected soils at Kurdistan region, north of Iraq. Iraqi J. Agri. Sci. 52(6) 1498-1507. https://doi.org/10.36103/ijas.v52i6.1491

Fayyadh MA, Rekani SAF (2022). Distribution path of total and active carbonates, and iron oxides under two different forest tree species. *In: IOP Conference Series: Earth and Environmental Science,* 1120 (1): 012038.

Friedman JH (2001). Greedy function approximation: A gradient boosting machine. Ann. Stat. 29(5): 1189-1232.

Gökmen V, Sürücü A, Budak M, Bilgili AV (2023). Modeling and mapping the spatial variability of

soil micronutrients in the Tigris basin. J. King Saud Univ.-Sci. 35(6): 102724. https://doi.org/10.1016/j.jksus.2023.102724

Hao Y, Yang Y, Liu B, Liu Y, Gao X, Guo Q (2016). Size characteristics of sediments eroded from three soils in China under natural rainfall. J. Soils Sed. 16(8): 2153-2165. https://doi.org/10.1007/s11368-016-1424-3

Hillel D (1998). *Environmental Soil Physics.* Academic Press. San Diego, CA.

Hudson BD (1994). Soil organic matter and available water capacity. J. Soil Water Conser. 49(2): 189-194. https://doi.org/10.1080/00224561.1994.12456850

Isaaks EH, Srivastava RM (1989). *An Introduction to Applied Geostatistics*. Oxford University Press.

Isaboke J, Osano O, Humphrey OS, Dowell SM, Njoroge R, Watts MJ (2025). Influence of agricultural land use management on soil particle size distribution and nutrient adsorption in Western Kenya. Chem. Africa 8(4): 1599-1610.

Jackson ML (1973). *Soil chemical analysis,* Pentice hall of India Pvt. Ltd., New Delhi, India, 498:151-154.

Johnson GV, Fixen PE (1990). Testing soils for sulfur, boron, molybdenum, and chlorine. Soil Test. Plant Ana. 3: 265-273. https://doi.org/10.2136/sssabookser3.3ed.c10

Jones C, Jacobsen J (2005). Plant nutrition and soil fertility. *Nutrient management module,* 2(11): 1-11.

Jolliffe I (2011). Principal component analysis. In: International encyclopedia of statistical science. Springer, Berlin, Heidelberg**:** 1094-1096.

Kerry R Oliver MA (2007). The analysis of ranked observations of soil structure using indicator geostatistics. Geoderma 140(4):397-416. https://doi.org/10.1016/j.geoderma.2007.04.020

Keshavarzi A, Sarmadian F, Ayoubi S (2020). Digital mapping of soil fertility using fuzzy logic and remote sensing data. Geoderma 361: 114061. https://doi.org/10.1016/j.geoderma.2019.114061

Khudher SA, Alkhaled KA (2024). Study of some fertility characteristics of soils with different agricultural uses in the Aqra Region/Duhok. World J. Adv. Res. Rev. 21(02): 301–312. https://doi.org/10.30574/wjarr.2024.21.2.0409

Kopittke PM, Harper SM,Asio LG, Asio VB, Batalon JT, Batuigas AMT, Sanchez PB (2025). Soil degradation: An integrated model of the causes and drivers. Int. Soil Water Conser. Res. 13: 744-755. https://doi.org/10.1016/j.iswcr.2025.07.010

Kumar Y, Srivastava SC, Gupta D, Singh W, Pandey AK, Arora D (2025). Analysis of soil fertility reduction using AI techniques: Opportunities and challenges. In: AIP Conference Proceedings (Vol. 3297, No. 1, p. 030008). AIP Publishing LLC. https://doi.org/10.1063/5.0287014

Lal R (2021). Soil organic matter and water retention. Agron. J. 112(5): 3265–3277. https://doi.org/10.1002/agj2.20282

Landon JR (1991). Booker Tropical Soil Manual: A Handbook for Soil Survey and Agricultural Land Evaluation in the Tropics and Subtropics (1st Ed.). Routledge. https://doi.org/10.4324/9781315846842

Li W (2022). Applications of machine learning in soil fertility evaluation and mapping. Geoderma 409: 115626. DOI: 10.1016/j.geoderma.2022.115626

Louzada RO, Bergier I, Bolfe ÉL, Barbedo JGA (2025). Integrating GIS and remote sensing for soil attributes mapping in degraded pastures of the Brazilian Cerrado. Soil Adv. 3: 100044. https://doi.org/10.1016/j.soilad.2025.100044

Magdic I, SafnerT, Rubinić V, Rutić F, Husnjak S, Filipović V (2022). Effect of slope position on soil properties and soil moisture regime of Stagnosol in the vineyard. J. Hydrol. Hydromech. 70(1): 62-73. https://doi.org/10.2478/johh-2021-0037

Matar AE (1992). Soil testing as a guide to fertilization in West Asia and North African (WANA) region. Commun. Soil Sci. Plant Ana. 23(17-20): 2075-2085. https://doi.org/10.1080/00103629209368725

Morais MA, de Andrade, AM, Junior JM (2021). Portable X-ray fluorescence spectrometry and artificial intelligence for rapid soil fertility assessment. Comp. Electron. Agri. 186: 106189. https://doi.org/10.1016/j.compag.2021.106189

Nigussie A, Ambaw G, Kissi E (2013.) Fertility status of Eutric Nitisol and fertilizer recommendation using NuMass in the selected areas of Jimma zone, Southwestern Ethiopia. Trop. Subtrop. Agroecosys.16: 487-495. DOI: 10.56369/tsaes.1425

Pedregosa F, Varoquaux, G, Gramfort A, Michel V, Thirion B, Grisel O, Duchesnay É (2011). Scikit-learn: Machine learning in Python. J. Machine Learning Res. 12: 2825-2830.

Razvanchy HAS, Fayyadh MA (2022). Application of geospatial techniques in analyst distribution pattern of some soil properties in Erbil Province, Kurdistan Region- Iraq. *J. Duhok Univ. 25(1):* 26-37.

Rekani SI, Al-Qazili, MS, Al-Obaidi MJ (2022). The Inclusive in Soil, Plant, Water and Fertilizer Analysis, text books. Dar Dijla, Amman, Jordan. (In Arabic)

Rodriguez-Galiano V (2012). Machine learning tools for environmental feature selection and modeling. Environ. Model. Software 37: 1-6. DOI: 10.1016/j.envsoft.2012.03.012

Rodrigues RR, Padgurschi, MCG, Ivanauskas NM, Teixeira AP, Lima RAF, Assis MA (2021). Topographic variability as a key driver of soil fertility in Atlantic forest ecosystems. Ecological Proc. 10: 33. https://doi.org/10.1186/s13717-021-00333-1

Singh KN, Rathore A, Tripathi AK, Subba Rao A, Khan S (2010). Soil fertility manning and its validation using spatial prediction techniques. J. Ind. Soc. Agri. Stat. 64: 359-365. URI: http://oar.icrisat.org/id/eprint/158

Singh SK, Pandey PC, Petropoulos GP (2021). Soil fertility mapping using GIS and remote sensing: A review on approaches, applications, and future perspectives. Remote Sen. Appl.: Soc. Environ. 22, 100493. https://doi.org/10.1016/j.rsase.2021.100493

Six J, Elliott ET, Paustian K (2000). Soil macroaggregate turnover and microaggregate formation: A mechanism for C sequestration under no-tillage agriculture. Soil Bio. Biochem. 32(14): 2099–2103. https://doi.org/10.1016/S0038-0717(00)00179-6

Soltanpour PN (1985). Use of ammonium bicarbonate DTPA soil test to evaluate elemental availability and toxicity. Commun. Soil Sci. Plant Ana. 16(3): 323-338. https://doi.org/10.1080/00103628509367607

Vaysse K, Heuvelink GB, Lagacherie P (2017). Spatial aggregation of soil property predictions in support of local land management. Soil Use Manage. 33(2): 299-310. https://doi.org/10.1111/sum.12350

Wang Y, Zhang X, Shi X (2023). Rapid estimation of soil properties using VNIR spectroscopy and machine learning. Remote Sen. 15(2): 311. https://doi.org/10.1016/j.jksus.2023.102724

Webster R (2001). Statistics to support soil research and their presentation. Europ. J. Soil Sci. 52(2): 331-340. https://doi.org/10.1046/j.1365-2389.2001.00374.x

Webster R, Oliver MA (2007). Geostatistics for Environmental Scientists. John Wiley & Sons.

Xing Y, Wang X, Mustafa A (2025). Exploring the link between soil health and crop productivity. Ecotoxicol. Environ. Saf. 289: 117703. https://doi.org/10.1016/j.ecoenv.2025.117703

Zeraatpisheh M, Ayoubi S, Jafari A (2020). Predicting soil fertility using machine learning algorithms in arid and semi-arid regions. Catena 190: 104543. https://doi.org/10.1016/j.catena.2020.104543

Zhang Y, Liu Y, Wu B (2018). Review of soil fertility indices and models for sustainable development in agriculture. Environ. Sci. Poll. Res. 25(21): 20568-20580. https://doi.org/10.1007/s11356-018-2437-0

Zhang Z, Zhu L (2023). A review on unmanned aerial vehicle remote sensing: Platforms, sensors, data processing methods, and applications. Drones 7(6): 398. https://doi.org/10.3390/drones7060398

Zhou T, Shi, X, Li, C, Yu D, Wang J (2020). Mapping soil fertility using geostatistical approaches in combination with remote sensing data. Catena 190: 104531. https://doi.org/10.1016/j.catena.2020.104531

Zhou W, Peng, J, Li H, Wang Y (2024). Effects of land use and slope position on the spatial distribution of soil nutrients. Geod. Reg. 32: e00654. https://doi.org/10.1016/j.geodrs.2023.e00654

Zhou Y, Zhao X, Guo X, Li Y (2022). Mapping of soil organic carbon using machine learning models: Combination of optical and radar remote sensing data. Soil Sci. Soc. Amer. J. 86(2): 293-310. https://doi.org/10.1002/saj2.20371.